Improving Seakeeping Performance of Fishing Boats by Minimising Radius of Gyration

Muhammad Iqbal[1,2], Momchil Terziev[1], Tahsin Tezdogan[3], Atilla Incecik[1]

1) Department of Naval Architecture, Ocean, and Marine Engineering, University of Strathclyde, Glasgow - G4 0LZ, UK
2) Department of Naval Architecture, Diponegoro University, Semarang – 50275, Indonesia
3) Department of Civil, Maritime and Environmental Engineering, University of Southampton, Southampton, UK

Abstract

Since the mortality rate of fishing at sea is the highest compared to other occupations in the world, improving the seakeeping performance is essential to enhance the safety of fishing vessels. One approach is to conduct seakeeping optimisation, which typically involves multiple objective functions. This study simplifies the objective function in seakeeping optimisation by using a single objective function: the Radius of Gyration in the Y direction (Ry), while varying the Longitudinal Centre of Gravity (LCG) and the Vertical Centre of Gravity (KG) positions as design variables. A Central Composite Design was employed to generate sample data, enabling the construction of a mathematical model and the identification of the optimal solution using Response Surface Methodology. The initial and optimal results, based on CFD simulation, were compared. The findings reveal that the optimum design variables in Ry, can enhance seakeeping at certain wavelength ratios, resulting in a lower RAO value compared to the initial condition. Furthermore, the influence of the design variables on total resistance (RT) was investigated. The results demonstrate that the seakeeping optimum has no significant impact on total resistance, as the difference with the optimum design for RT and the initial condition is very low, predicted to be no more than 0.5%. This discovery suggests that minimising Ry can improve seakeeping without significantly affecting total resistance.

Key words: Small Fishing Boat, GM Ratio, Seakeeping, Added Resistance, Response Surface Method

1. Introduction

Consuming fish is essential for humans and is also aligned with Sustainable Development Goals number 2 and 3, which aim to eradicate hunger and ensure a healthy life for all. However, ensuring that people can consume fish, fishermen are exposed to significant risks, as fishing at sea is considered the most dangerous occupation in the world. [1]. The mortality rate in fishing surpasses that of other occupations. Numerous accidents occur during sea fishing, particularly for small fishing vessels [2], [3]. Therefore, research aimed at enhancing safety for fishing vessels is crucial.

One of the contributing factors to accidents is environmental conditions. Poor weather, strong winds, and high waves hinder the operation of fishing boats, leading to a low operability index [4]. Ensuring that fishing boats can operate effectively in their designated areas can minimise the risk of accidents. This can be achieved by enhancing the seakeeping performance of the fishing vessel.

The nature of fishing vessels entails that their loading conditions constantly fluctuate. Upon departure from the shore, the fish tank is empty, gradually increasing in payload based on the number of fish caught during operation. Moreover, the method of fishing and the placement of fish onboard can alter the centre of gravity (CoG), both longitudinally and vertically, thereby affecting stability in waves and potentially triggering the parametric roll phenomenon due to changes in GM and natural period.

Another consequence of the shifting CoG position is its impact on the Moment of Inertia in the Y-axis (Iyy), consequently influencing the Radius of Gyration in the Y-axis (Ry), as illustrated in Eq. 1. With constant displacement, minimising Ry can also minimise Iyy. Since the hull shape remains unchanged, both the damping coefficient (C) and the added moment of inertia in the Y-axis (Iyy(a)) can be considered constant. The change in natural frequency, ω_n, which is relatively small compared to the changes in total Iyy, makes a vessel with a lower Ry exhibits lower critical damping, resulting in a higher pitch damping ratio (ζ), as depicted in Eq. 2. A higher pitch damping ratio helps minimise pitch amplitude.

$$R_y = \sqrt{\frac{I_{yy}}{\Delta}} = \sqrt{\frac{\sum w_i({z_i}^2 + {x_i}^2)}{\Delta}} \quad \text{Eq. 1}$$

$$\zeta = \frac{C}{C_r} = \frac{C}{2(I_{yy} + I_{yy(a)})\omega_n} \quad \text{Eq. 2}$$

Most literature utilises individual ship responses as objective functions for seakeeping optimisation, including heave, pitch, and roll. [5], [6], with additional objective function such as vertical or (and) lateral acceleration [7], [8], [9] slamming [10], or motion sickness incidence [11]. Thus, to enhance seakeeping, it becomes necessary to minimise all responses, which complicates the optimisation process as multiple objective functions are required.

The research aims to demonstrate the utilisation of Ry as a single objective function to indirectly improve seakeeping performance and to streamline the seakeeping optimisation process by altering the loading position (LCG and KG), inherent to the nature of fishing vessel operation. The Response Amplitude Operator (RAO) in heave, pitch, and added resistance of both initial and optimum conditions are then compared, as predicted by the URANS CFD method.

Furthermore, the present study also investigates the influence of design variables, LCG and KG, on calm water resistance. A same optimisation procedure to minimise calm water resistance is used and the impact of both design variables on total resistance is investigated.

2. Methodology

2.1. Subject Ship and Simulation Condition

In this paper, a small fishing vessel called FAO-01 is employed based on Pérez-Arribas et al. [12]. CFD simulations were reported by Díaz-Ojeda et al. [13] and compared with the experimental test data. They utilised a dihedral bulbous bow for this fishing vessel to

reduce the total resistance in calm water. The results of experimental tests on resistance were presented on a scale factor of 4 at Fr 0.33. The main dimensions are shown in **Table 1**, while the lines plan is presented in **Figure 1**. For the CFD simulation in waves, simulations were conducted by varying the wavelength ratio, λ/Lbp, from 1.15 to 3.0. H/λ was set to 0.06 for the wave height across all wavelengths, and Fr = 0.33 was maintained for the forward speed.

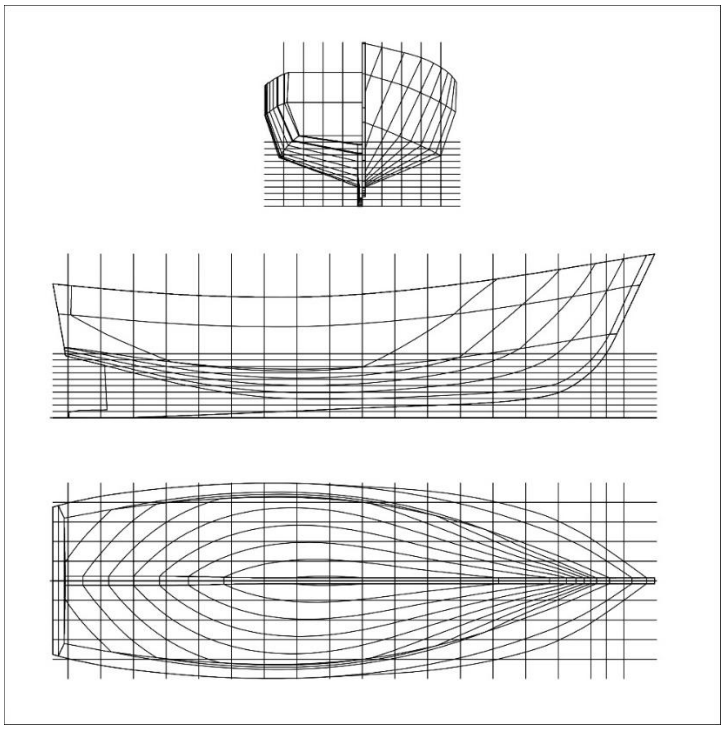

Figure 1. Lines plan of subject ship, FAO-01

Table 1. Main dimensions of FAO-01 fishing vessel

Parameter	Value
Length overall, LOA (m)	9.232
Breadth moulded, B (m)	3.00
Depth moulded, D (m)	1.14
Loaded draft, T (m)	0.983
Volume Displacement, $\Delta(m^3)$	5.846
Block coefficient, C_b (-)	0.267
Mid-boat section coefficient, Cm (-)	0.525
Wetted surface area, Aw (m^2)	23.914

The accuracy of the CFD model was assessed by comparing the CFD results with the experimental data. As the fishing boat only provided resistance data, the well-known benchmark for seakeeping tests of the KCS model, based on Simonsen et al. [14], was utilised. Subsequently, the methodology for setting up the CFD seakeeping simulation was applied to the fishing boat. Meanwhile, the Grid Convergence Index (GCI), based on Roache [15], was employed for the uncertainty study of the CFD model.

2.2. Optimisation Procedure

The optimisation procedure in this study began with determining the objective function and the design variables. As mentioned in the Introduction section, a novel objective function, Ry, was utilised, while LCG and KG served as the design variables.

Following this, the Central Composite Design (CCD), as illustrated in Figure 2, was employed as a Design of Experiment (DoE) to systematically gather sample data [16]. In Figure 2, nine variations resulted from the combination of two variables (x1 and x2). Since the units of each variable are not the same, they were converted to 1 and -1 to represent the maximum and minimum changes in each variable, respectively, determined by ±5% changes from the initial value as shown in Table 2. The code of ±1.414 in Figure 2 corresponds to fractional factorial designs, specifically tailored for two-level factorial experiments involving two design variables, which can be determined by linear extrapolation between 0 and 1.

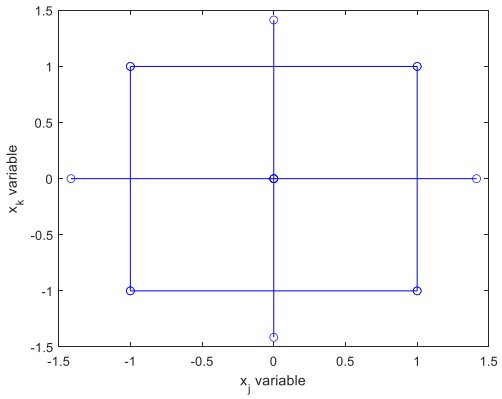

Figure 2. Central Composite Design for Design of Experiment

Table 2. Initial, Maximum, and Minimum Design Variable

Design Variable	FAO-01		
	-1	**0**	**1**
LCG (m), $\boldsymbol{x_1}$	0.898	0.945	0.992
KG (m), $\boldsymbol{x_2}$	0.360	0.379	0.398

$$y_i(x_j, x_k) = a + bx_j + cx_k + dx_j{}^2 + ex_k{}^2 + fx_jx_k \quad \text{Eq. 3}$$

$$y_{i\,max/min}(x_j, x_k) = \frac{dy_i(x_j, x_k)}{dx_j} \quad \text{Eq. 4}$$

$$y_{i\,max/min}(x_j, x_k) = \frac{dy_i(x_j, x_k)}{dx_k}$$

In **Table 2**, LCG is measured from AP, and KG is measured from the baseline. The initial LCG is assumed to be the same value as LCB, which ensures the vessels are on an even keel. Meanwhile, the initial KG is assumed to be 75% of KM. Subsequently, based on the responses from each sample data, a mathematical model can be constructed to identify the

minimum location of the response, in this case, Ry. This is achieved by employing regression analysis for two variables, as shown in Eq. 3. Then, the optimal solution can be determined from the first derivative with respect to each variable (j, k), as shown in Eq. 4.

2.3. Numerical Simulation

The Unsteady Reynolds Averaged Navier-Stokes (URANS) CFD method was employed to determine the response of heave and pitch, as well as the total resistance in waves for different wavelength ratios. This method has been favoured by numerous researchers, including Guan et al. [17], Zhang et al. [18] and Miao et al. [19], due to its ability to incorporate viscous effects into seakeeping performance, which are neglected in Potential Theory-based methods. By including the viscous term, the accuracy of the predicted ship response becomes significantly improved.

In this case, Star CCM+ software version 17.04 was utilised, which employs the finite volume method to discretise the governing equations. The convection term was solved using a second-order convection scheme, and the unsteady term utilised the implicit method. Velocity and pressure were solved using the Semi-Implicit Method for Pressure Linked Equations (SIMPLE) algorithm. The k-ε turbulence model was selected as the turbulence model.

The free surface was captured using the volume fraction method, assigning a scalar value between 0 to 1 in each cell to represent water and air. The location of the free surface can then be identified simply by a scalar value of 0.5. To model motions, Star CCM+ offers a module called Dynamic Fluid Body Interaction (DFBI). This module enables the calculation of the force and moment on the hull and then calculates the motion equation to determine the new position in a new time step.

The computational domain spans from -3LOA to 2.3LOA in length and from -1.5 LOA to 1 LOA in height. Since the seakeeping simulation uses head waves, only half of the computational domain is required, resulting in a width of computational domain spanning from 0 to 1.5 LOA. The boundary condition where the centre line of the ship is located was set as symmetry. The downstream location was set as a pressure outlet to maintain the hydrostatic pressure. The remaining boundaries were set as velocity inlets, including the upstream location. Here, the VOF Wave Module for Star CCM was utilised at each velocity inlet to model a 'flat wave' for calm water resistance simulation and to model fifth-order waves for seakeeping simulation.

The mesh was generated using the cartesian cut-cell method automatically offered by Star CCM+. In this simulation, an overset mesh was employed, dividing the mesh into two regions: background and overset. At least two refinements were implemented for each region, located at the boundary layer and free surface. At the boundary layer, the first layer height was determined based on the targeted y+, which in this study was targeted between 30 to 100 [20].

$$\lambda = \frac{2\pi}{k} = \frac{2\pi}{(g/V^2)} \qquad \text{Eq. 5}$$

$$\Delta t = 0.005 - 0.01\,\frac{L}{V} \qquad \text{Eq. 6}$$

In calm water simulation, free surface refinement was initially carried out by determining the cell size in the Kelvin Wake region. This was achieved by calculating the wavelength

generated by the ship movement using Eq. 5, where V represents the ship speed in m/s and g is the gravitational acceleration. Subsequently, 24 cells were employed per λ for its length and width, while the height cell (z-direction) was determined by using 1/8 of the cell length. The rest of the free surface was then doubled from the Kelvin wake zone.

In the seakeeping simulation, the free surface refinement was carried out based on the ITTC recommendations, where at least 80 cells were employed per λ and 20 cells for wave height. This recommendation was applied for the lowest wavelength ratio, λ/Lbp = 1.15.

Finally, the determination of the time step utilised the ITTC recommendation, as shown in Eq. 6, where L represents the ship length in metres and V is the ship speed in m/s. For the seakeeping simulation, $T_e/2^8$ was used following the approach by Cho et al. [21], which is lower than the ITTC recommendation ($T_e/100$).

3. Results and Discussion

3.1. Accuracy and Numerical Uncertainty of CFD Model

Table 3 presents the accuracy study of the CFD model by comparing the results based on CFD and EFD. It is evident that the coefficient of total resistance in calm water has a slight difference, which is 1.06%. Meanwhile, in wave conditions, the Transfer Functions (TF) of heave, pitch, and added resistance are compared. The heave TF shows insignificant difference, while for pitch TF and added resistance TF, the difference is around 5%, which is considered acceptable. **Table 4** represents the comparison of CFD and EFD results for the calm water resistance of the fishing boat FAO-01. It can be observed that the difference is below one percent, indicating that the CFD result has a good agreement with experimental results.

Table 3. The comparison of CFD and EFD results for calm water resistances and wave condition of the KCS model.

Method	Calm Water	Wave Condition (λ/Lbp = 1.15)		
	CT (*103)	Heave TF	Pitch TF	Added Resistance TF
EFD [14]	4.31	0.950	0.693	9.106
Present CFD	4.36	0.954	0.727	9.564
Difference (%)	1.06%	0.43%	4.89%	5.03%

Table 4. The comparison of CFD and EFD results for calm water resistances of FAO-01 Fishing Vessel

Method	RT (N)
EFD [13]	15.310
Present CFD	15.162
Difference (%)	-0.97%

The uncertainty study for the CFD model was investigated using the Grid Convergence Index (GCI), which required three configurations: fine, medium, and coarse. The CFD set-up for which the results are shown in Table 3 and Table 4 is referred to as the fine configuration. Subsequently, the fine configurations were coarsened into medium and coarse configurations using a refinement ratio.

For the KCS model, a refinement ratio of $\sqrt{2}$ was used to coarsen the fine to medium configuration. Then, with the same ratio, the medium configuration was coarsened again into the coarse configuration. For the fishing boat FAO-01, refinement factors of 1.23 and

1.24 were used to coarsen the fine to medium and medium to coarse configurations, respectively.

Table 5. GCI results of the KCS model

Parameters	**CT Calm Water**	**Wave Condition (λ/Lbp = 1.15)**		
	CT (*103)	**Heave TF**	**Pitch TF**	**Added resistance TF**
Fine Configuration	total cell = 3,591,024 time step = 0.01845 s	total cell = 4,330,069 time step = 0.00360 s		
Medium Configuration	total cell = 1,396,929 time step = 0.02609 s	total cell = 1,889,342 time step = 0.00509 s		
Coarse Configuration	total cell = 561,609 time step = 0.03690 s	total cell = 923,707 time step = 0.00720 s		
Fine solution, S_1	0.00436	0.9541	0.7269	9.5638
Medium solution, S_2	0.00444	0.9550	0.7265	9.8579
Coarse solution, S_3	0.00458	0.9650	0.7131	15.2748
GCI (%)	3.05810	0.0117	0.0021	0.2207

Table 6. GCI Results of FAO-01 Fishing Vessel

Parameters	**RT Calm Water**	**Wave Condition (λ/Lbp = 1.5)**		
		Heave TF	**Pitch TF**	**Added resistance TF**
Fine Configuration	total cells = 1,715,717 time step = 0.0131 s	total cell = 3,536,648 time step = 0.0026 s		
Medium Configuration	total cells = 1,010,918 time step = 0.0161 s	total cell = 1,419,264 time step = 0.0037 s		
Coarse Configuration	total cells = 577,607time step = 0.0200 s	total cell = 512,760 time step = 0.0052 s		
Fine solution, S_1	15.1616 N	1.1177	0.6884	1.9716
Medium solution, S_2	15.5010 N	1.1157	0.6837	1.9473
Coarse solution, S_3	16.2236 N	1.0937	0.6657	1.8631
GCI (%)	2.7495	0.0224	0.3016	0.6250

Table 5 illustrates the GCI results of the KCS model. It is evident that the GCI result for CT is higher than the result for seakeeping simulations, which is less than 1%. However, the GCI for CT is considered acceptable as it is under 5%. A similar trend is observed with the FAO-01, where the GCI for seakeeping simulation is less than one percent, while for the total resistance in calm water, it is around 2.75%.

Based on the accuracy and numerical uncertainty studies conducted, it is evident that the CFD models have yielded good results. Therefore, the CFD results in this study are deemed reliable for further analysis in the following sections.

3.2. Optimisation Results

Table 7 illustrates the Ry response of the FAO-01 fishing boat based on Central Composite Data. The responses are represented by the Calculated Ry (Ry Cal) calculated using Rhinoceros software. All the responses were utilised to construct a mathematical model, as mentioned in section 2.2, and the result of the equation is presented in Eq. 7. This regression equation has an R2 value of 0.9998, indicating that LCG and KG significantly influence the Ry up to 99.98%. Subsequently, the Ry result based on Rhinoceros (Ry Cal) and Ry based on Eq. 7 (Ry Eq. 7) were compared in **Table 7**. The error between them is also presented in the same table with a maximum absolute value of 0.01%. Therefore, Eq. 7 is sufficiently accurate to be used in this optimisation process.

Table 7. The R_y response of FAO-01 fishing boat based on Central Composite Design

Load Case	X1	X2	LCG (m)	KG (m)	Ry Cal (m)	Ry Eq. 7 (m)	Error (%)
Initial	0	0	0.945	0.379	0.55330	0.55330	0.00%
LC 1	1	1	0.992	0.398	0.55700	0.55701	0.00%
LC 2	1	-1	0.992	0.360	0.55390	0.55386	0.01%
LC 3	-1	1	0.898	0.398	0.55750	0.55754	-0.01%
LC 4	-1	-1	0.898	0.360	0.55430	0.55429	0.00%
LC 5	-1.414	0	0.878	0.379	0.55770	0.55768	0.00%
LC 6	1.414	0	1.012	0.379	0.55700	0.55702	0.00%
LC 7	0	-1.414	0.945	0.352	0.55170	0.55174	-0.01%
LC 8	0	1.414	0.945	0.406	0.55630	0.55626	0.01%

$$Ry\ (m) = 0.5533 - 0.0002x_1 + 0.0016x_2 + 0.0020{x_1}^2 + 0.0003{x_2}^2 \quad \text{Eq. 7}$$

The visualisation of Eq. 7, known as the response surface, is depicted in Figure 3. From the figure, it is evident how LCG and KG influence Ry. To minimise Ry, it is advisable to maintain LCG as close to the initial condition as possible, while KG should be decreased from the initial setting. The rectangle shown in the figure represents a constraint, ensuring that the optimum design variables are feasible for implementation. The constraint codes are set as ±2.5, indicating ±12.5% changes from the initial value. Therefore, the minimum location should be identified inside this rectangle. Finally, the minimum Ry location is denoted by a point in Figure 3, with the LCG code at 0.05 and the KG code at -2.5.

Table 8 presents the comparison between the initial and optimum Ry, both in code and real value. Subsequently, the Ry value based on the calculation and Eq. 7can be determined and compared to the initial condition. According to the prediction (Eq. 7), the Ry value can reduce by 0.332% when LCG and KG are positioned optimally. Meanwhile, based on the calculation, optimum LCG and KG can reduce Ry from the initial condition by up to 0.352%. The prediction result has a slight difference with the calculations due to the high accuracy of the mathematical model, which is represented by the R2 value. Once the optimum results have been determined, the optimization process is concluded.

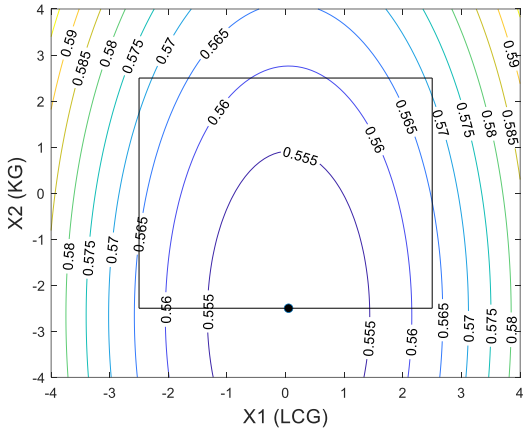

Figure 3. Response Surface Result for R_y Influenced by LCG and KG with the constrains and optimal location

Table 8. The comparison between initial and optimum R_y

Load Case	x_1	x_2	LCG (m)	KG (m)	Ry Cal (m)	Ry Eq. 7 (m)
Initial	0.00	0.00	0.945	0.379	0.55330	0.55330
LC 9 (Optimum Ry)	0.05	-2.50	0.947	0.332	0.55136	0.55147
Difference (%)					-0.351%	-0.332%

3.3. Seakeeping Performance in Regular Waves

The next step is to conduct seakeeping simulations, as described in section 2.2, for both initial and optimum conditions to be compared. Fast Fourier Transformation was employed to determine the heave and pitch amplitude as well as the mean total wave resistance. Finally, each ship response in regular waves is converted to a transfer function (TF), as shown in Eq. 8 to Eq. 10.

$$Heave\ TF = \frac{z_a\ (m)}{\zeta\ (m)} \quad \text{Eq. 8}$$

$$Pitch\ TF = \frac{\theta_a\ (rad)}{k\zeta\ (rad)} \quad \text{Eq. 9}$$

$$Added\ Resistance\ TF = \frac{RT_{wave} - RT_{calm}\ (N)}{\rho g \zeta^{\,2} B^2/L\ (N)} \quad \text{Eq. 10}$$

Transfer functions resulting from each wavelength ratio (λ/Lbp) were then plotted to construct the Response Amplitude Operator (RAO), as depicted in **Figure 4**. From the figure, it is clear that minimising Ry can reduce the amplitude of heave and pitch at certain wavelength ratios. For heave and added resistance, the TF begins to decrease from λ/Lbp of 2, while pitch starts from 2.5.

It can be concluded that minimising Ry has an impact on the seakeeping performance. The optimisation process can be considered successful as the optimum design variables can be determined and minimum Ry can be achieved. As the RAO curve is a representation of ship response in regular waves, further investigation is needed to determine ship responses in

irregular waves, which represent its performance in its operational area. However, this investigation is not included in this paper. Instead, that is left as a piece of future work.

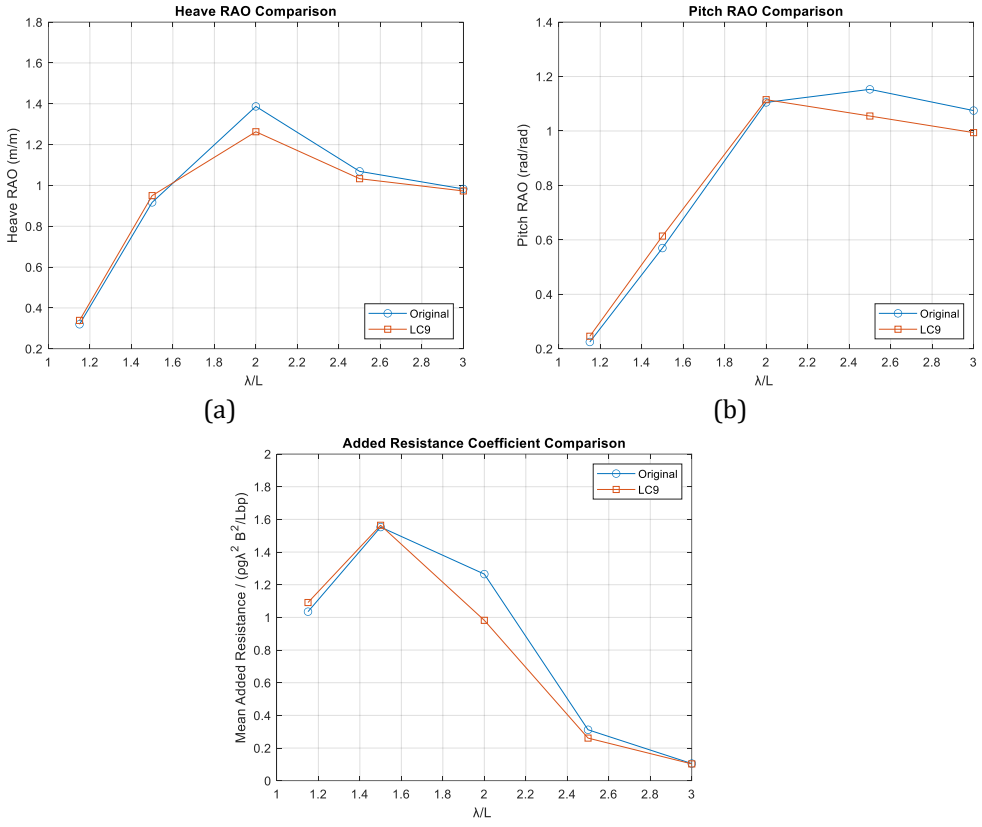

Figure 4. The heave, pitch, and added resistance RAO comparison between initial and optimum condition

Figure 5 illustrates the comparison of wave elevations for initial and optimum conditions. The differences between both conditions can be observed qualitatively by comparing the wake generated by the vessel movement. The wake generated by LC 9 (optimum condition) is lower than the initial condition, indicating that the vessel has lower amplitude or responses in the same wave condition.

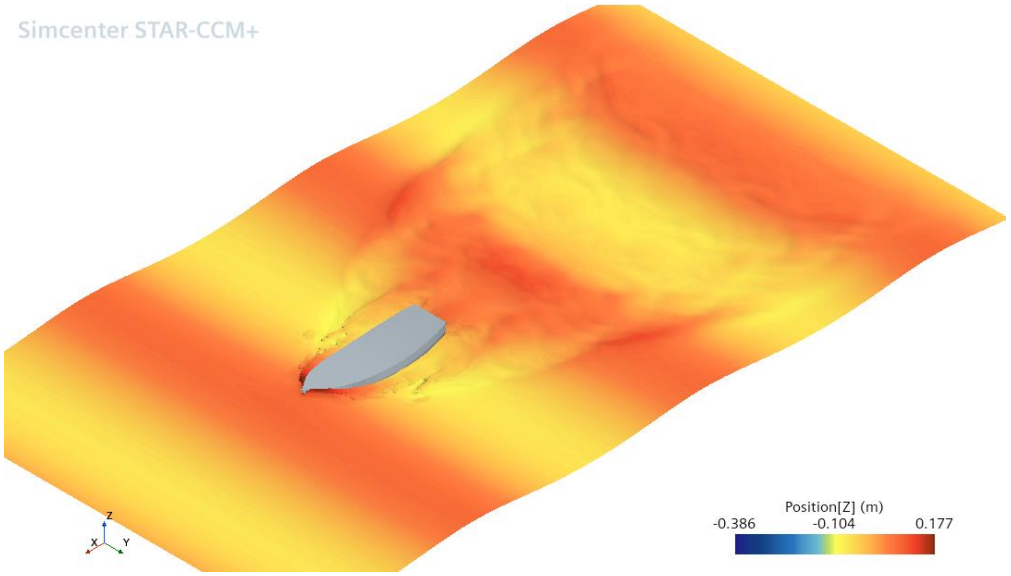

(a) Initial Condition

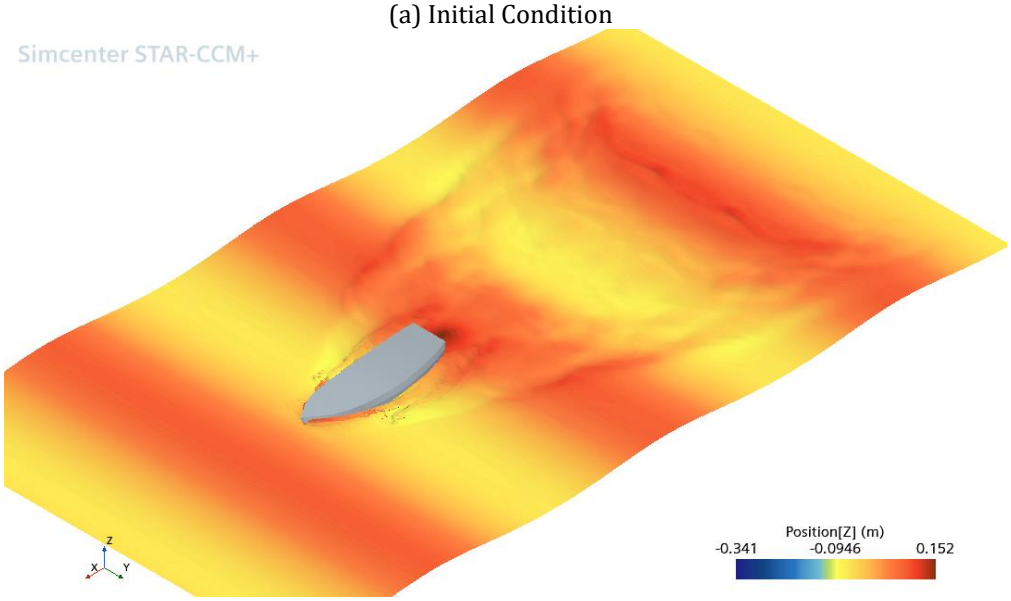

(b) LC 9

Figure 5. The result of CFD seakeeping simulation at λ/Lbp = 2

3.4. The Influence of LCG and KG to Calm Water Resistance

The previous section concluded that LCG and KG have an impact on the Ry value, which indirectly influences the seakeeping performance. This paper attempts to investigate both parameters' influence on total resistance in calm water by applying the same optimisation process. Based on the resulting mathematical model as well as the response surface figure, the influence of LCG and KG on the total resistance in calm water can be clearly observed.

Table 9 presents the total resistance for each load case variation based on Central Composite Design in Figure 2. The data were then used to construct the mathematical model, as shown in Eq. 8, which has an R2 value of 0.9757. According to the mathematical

model, the total resistance of FAO-01 is influenced as much as 97.57% by LCG and KG. The remaining 2.5% represents an unknown factor that also influences the total resistance.

In Table 9, the comparison between predicted RT (RT Eq. 8) and CFD-based RT (RT CFD) shows a slightly higher value compared to the Ry result in Table 7. The maximum error reaches 0.2%, which is still below 1% and considered acceptable. The predicted results will have slightly different values compared to the actual results, as shown in Table 8.

Table 9. The RT response of FAO-01 fishing boat based on Central Composite Design

Load Case	X1	X2	LCG	KG	RT CFD (N)	RT Eq. 8 (N)	Error (%)
Original	0	0	0.945	0.379	15.162	15.162	0.00%
LC 1	1	1	0.992	0.398	15.225	15.217	0.05%
LC 2	1	-1	0.992	0.360	15.253	15.223	0.20%
LC 3	-1	1	0.898	0.398	15.316	15.340	-0.15%
LC 4	-1	-1	0.898	0.360	15.397	15.398	-0.01%
LC 5	-1.414	0	0.878	0.379	15.543	15.524	0.12%
LC 6	1.414	0	1.012	0.379	15.287	15.313	-0.17%
LC 7	0	-1.414	0.945	0.352	15.174	15.193	-0.13%
LC 8	0	1.414	0.945	0.406	15.160	15.148	0.08%

$$RT\ (N) = 15.162 - 0.0746x_1 - 0.0161x_2 + 0.1282{x_1}^2 + 0.0042{x_2}^2 + 0.0132x_1x_2 \quad \text{Eq. 11}$$

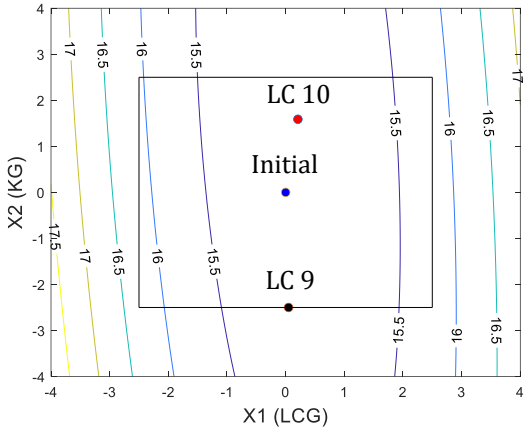

Figure 6. Response Surface Result for RT Influenced by LCG and KG with the constrains and optimal location

Figure 6 illustrates the location of the optimum LCG and KG for total resistance (LC 10), as well as their impact on total resistance represented by red points. Unlike the Ry response, it can be observed that KG has no significant impact compared to LCG towards the RT response. However, the optimum KG is located higher than the initial KG, while the optimal LCG is situated around the initial condition.

The figure also compares LC 9 (optimum LCG and KG for Ry) represented by black points, for the predicted total resistance. Based on Eq. 8, LC 9 has a total resistance of 15.223, which is predicted to be 0.54% higher than LC 10 and 0.4% higher than the initial condition. This indicates that the improvement in seakeeping achieved by LC 9 has no significant impact on the total resistance in calm water.

Table 10. Comparison between initial and optimum RT

Load Case	x_1	x_2	LCG (m)	KG (m)	RT CFD (N)	RT Eq. 8 (N)
Original	0.00	0.00	0.945	0.379	15.162	15.162
LC 10 (Optimum RT)	0.209	1.588	0.955	0.409	15.173	15.141
Difference (%)					0.073%	-0.136%

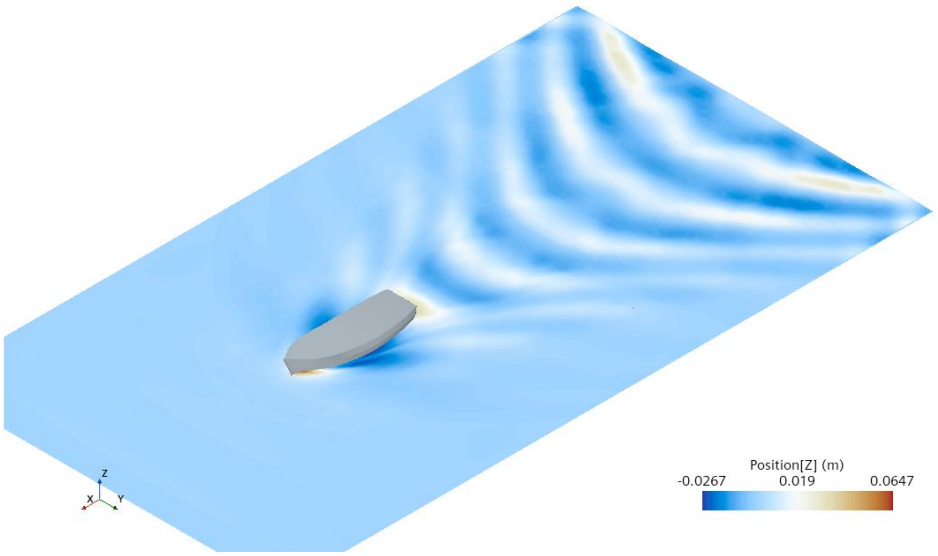

(a) Initial Condition

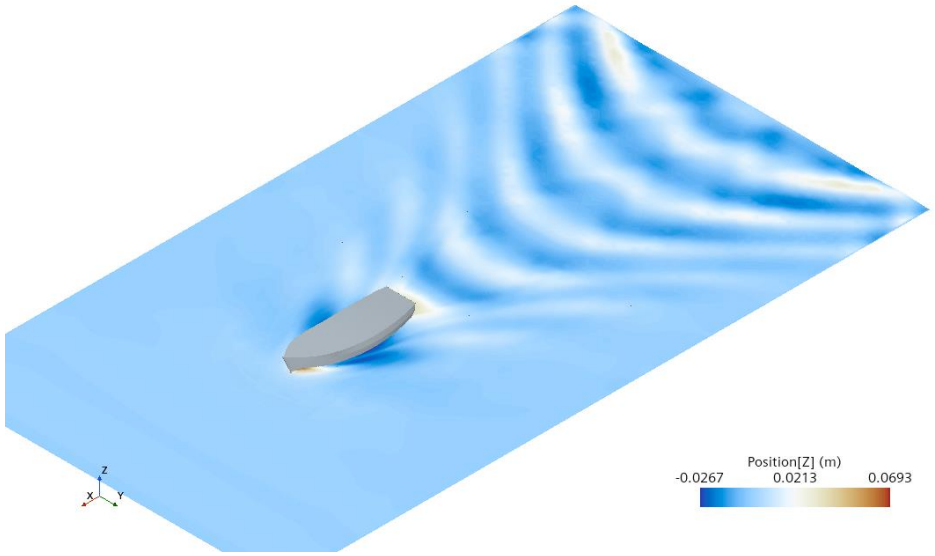

(b) LC 10

Figure 7. Result of CFD resistance simulation at Fr = 0.33

The comparison of total resistance in calm water between the initial condition and the optimum condition (LC 10) is shown in Table 10. It can be observed that, based on Eq. 8, the optimal LCG and KG can reduce the total resistance by up to 0.136%. This reduction is

minimal, as it is less than 1%. Additionally, the predicted result may have slightly different results compared to the actual value, which is CFD-based results, due to lower accuracy compared to the Ry optimisation.

When CFD simulation was carried out for the optimum load case (LC 10), the result was slightly higher than the predicted value, with a difference of 0.21%. This discrepancy is considered to have a low error. However, it was found that the optimum results had a slightly higher value of 0.073% compared to the initial condition, which once again indicates a negligible difference, lies in all cases within the predicted discretisation uncertainty obtained in Table 6. These findings suggest that there is no significant improvement in total resistance by changing LCG and KG. Further research is required to investigate the influence of hull form transformation on total resistance in calm water as well as seakeeping performance.

Finally, the CFD-based comparison between the initial and LC 10 results is presented in Figure 7. As the total resistance does not show a significant difference, the wave amplitudes inside the Kelvin wake also appear similar to the initial condition.

4. Conclusions

The radius of gyration in the y direction (Ry) was effectively demonstrated as a single objective function in the seakeeping optimisation process. LCG and KG were employed as design variables in the optimisation process. Seakeeping simulations were conducted using the CFD method, incorporating the viscous effect to enhance the results.

The optimal design variable in minimising Ry, known as LC 9, illustrates that the Response Amplitude Operator (RAO) of heave, pitch, and added resistance in head waves at Fr=0.33 can be reduced at certain wavelength ratios, thereby improving the seakeeping performance. The influence of the same design variables was successfully analysed, resulting in LC 10, which, as predicted by the mathematical model, can reduce the total resistance by up to 0.136%.

However, the CFD-based results for LC 10 showed an increase in total resistance by 0.073%, indicating that both design variables have no significant impact on total resistance. This finding also indicates that LC 9 exhibits no significant difference in total resistance compared to LC 10 (0.54% higher) and compared to the initial condition (0.4% higher). Improving seakeeping performance by minimising Ry can enhance seakeeping indirectly without significantly increasing the total resistance in calm water.

References

[1] FAO, *The State of World Fisheries and Aquaculture Part 2: Selected Issues Facing Fishers and Aquaculturists, the State of World Fisheries and Aquaculture*, vol. 3. Food & Agriculture Org., 2000.

[2] J. Wang, A. Pillay, Y. S. Kwon, A. D. Wall, and C. G. Loughran, “An analysis of fishing vessel accidents,” *Accident Analysis & Prevention*, vol. 37, no. 6, pp. 1019–1024, 2005.

[3] F. Ugurlu, S. Yildiz, M. Boran, Ö. Ugurlu, and J. Wang, “Analysis of fishing vessel accidents with Bayesian network and Chi-square methods,” *Ocean Engineering*, vol. 198, p. 106956, 2020.

[4] M. Iqbal, M. Terziev, T. Tezdogan, and A. Incecik, “Operability analysis of traditional small fishing boats in Indonesia with different loading conditions,” *Ships and Offshore Structures*, vol. 18, no. 7, pp. 1060–1079, Jul. 2023, doi: 10.1080/17445302.2022.2107300.

[5] N. K. Bales, “Optimizing the seakeeping performance of destroyer type hulls,” in

Published by: David W. Taylor Naval Ship Research \& Development Center, Ship Performance Department, Bethesda, Maryland, USA, Prepared for the 13th Symposium on Naval Hydrodynamics, ONR, Tokyo, Japan, 1980, 1980.

[6] S. M. Wang, S. Ma, and W. Y. Duan, "Seakeeping optimization of trimaran outrigger layout based on NSGA-II," *Applied Ocean Research*, vol. 78, pp. 110–122, Sep. 2018, doi: 10.1016/j.apor.2018.06.010.

[7] G. Ozmen, "Hull Form Optimisation of Fishing Vessels With Respect to Seakeeping," University of Glasgow (United Kingdom), 1995.

[8] L. Bagheri, H. Ghassemi, and A. Dehghanian, "Optimizing the seakeeping performance of ship hull forms using genetic algorithm," *TransNav: International Journal on Marine Navigation and Safety of Sea Transportation*, vol. 8, no. 1, pp. 49–57, 2014.

[9] G. Vernengo, S. Brizzolara, and D. Bruzzone, "Resistance and seakeeping optimization of a fast multihull passenger ferry," *International Journal of Offshore and Polar Engineering*, vol. 25, no. 01, pp. 26–34, 2015.

[10] E. Sarıöz, "Inverse design of ship hull forms for seakeeping," *Ocean Engineering*, vol. 36, no. 17–18, pp. 1386–1395, Dec. 2009, doi: 10.1016/j.oceaneng.2009.08.011.

[11] P. Romero-Tello, J. E. Gutierrez-Romero, and B. Serván-Camas, "Seakeeping optimization of cruise ship based on artificial neural networks," *Trends in Maritime Technology and Engineering*, pp. 435–441, 2022.

[12] F. Pérez-Arribas, A. Silva-Campillo, and H. R. D\'\iaz-Ojeda, "Design of Dihedral Bows: A New Type of Developable Added Bulbous Bows—Experimental Results," *Journal of Marine Science and Engineering*, vol. 10, no. 11, p. 1691, 2022.

[13] H. R. Díaz-Ojeda, F. Pérez-Arribas, and S. R. Turnock, "The influence of dihedral bulbous bows on the resistance of small fishing vessels: A numerical study," *Ocean Engineering*, vol. 281, p. 114661, 2023.

[14] C. D. Simonsen, J. F. Otzen, S. Joncquez, and F. Stern, "EFD and CFD for KCS heaving and pitching in regular head waves," *Journal of Marine Science and Technology*, vol. 18, pp. 435–459, 2013.

[15] P. J. Roache, *Verification and validation in computational science and engineering*, vol. 895. Hermosa Albuquerque, NM, 1998.

[16] R. Roy, S. Hinduja, and R. Teti, "Recent advances in engineering design optimisation: Challenges and future trends," *CIRP annals*, vol. 57, no. 2, pp. 697–715, 2008.

[17] G. Guan, L. Wang, J. Geng, Z. Zhuang, and Q. Yang, "Parametric automatic optimal design of USV hull form with respect to wave resistance and seakeeping," *Ocean Engineering*, vol. 235, p. 109462, Sep. 2021, doi: 10.1016/j.oceaneng.2021.109462.

[18] S. Zhang, T. Tezdogan, B. Zhang, L. Xu, and Y. Lai, "Hull form optimisation in waves based on CFD technique," *Ships and Offshore Structures*, vol. 13, no. 2, pp. 149–164, Feb. 2018, doi: 10.1080/17445302.2017.1347231.

[19] A. Miao, T. Chen, X. Qi, and D. Wan, "Multi-objective optimization design of KCS based on seakeeping performance," in *ISOPE International Ocean and Polar Engineering Conference*, 2018, p. ISOPE--I.

[20] M. Terziev, T. Tezdogan, and A. Incecik, "Scale effects and full-scale ship hydrodynamics: A review," *Ocean Engineering*, vol. 245, p. 110496, Feb. 2022, doi: 10.1016/j.oceaneng.2021.110496.

[21] J.-H. Cho, S.-H. Lee, D. Oh, and K.-J. Paik, "A numerical study on the added resistance and motion of a ship in bow quartering waves using a soft spring system," *Ocean Engineering*, vol. 280, p. 114620, 2023.